




Article

Assembled Porphyrin Nanofiber on the Surface of g-C₃N₄ Nanomaterials for Enhanced Photocatalytic Degradation of Organic Dyes

Hoan Thi Lai ¹, Giang Thi Nguyen ², Nga Thuy Tran ¹, Thanh Tung Nguyen ² , Chinh Van Tran ^{3,*},
Duy Khiem Nguyen ⁴, S. W. Chang ⁵, W. Jin Chung ⁵, Dinh Duc Nguyen ^{5,*} , Hoai Phuong Nguyen Thi ³
and Duong Duc La ^{3,*} 

- ¹ Department of Fundamental Science, University of Transport and Communications, Cau Giay, Dong Da, Hanoi 100000, Vietnam
- ² Institute of Materials Science, Vietnam Academy of Science and Technology, 18-Hoang Quoc Viet, Hanoi 100000, Vietnam
- ³ Institute of Chemistry and Materials, 17 Hoang Sam, Nghia Do, Cau Giay, Hanoi 100000, Vietnam
- ⁴ VN-UK Institute for Research and Executive Education, The University of Danang, Danang 550000, Vietnam
- ⁵ Department of Environmental Energy Engineering, Kyonggi University, Goyang 10285, Republic of Korea
- * Correspondence: chinhpkq@gmail.com (C.V.T.); nguyensyduc@gmail.com (D.D.N.); duc.duong.la@gmail.com (D.D.L.)



Citation: Lai, H.T.; Nguyen, G.T.; Tran, N.T.; Nguyen, T.T.; Van Tran, C.; Nguyen, D.K.; Chang, S.W.; Chung, W.J.; Nguyen, D.D.; Thi, H.P.N.; et al. Assembled Porphyrin Nanofiber on the Surface of g-C₃N₄ Nanomaterials for Enhanced Photocatalytic Degradation of Organic Dyes. *Catalysts* **2022**, *12*, 1630. <https://doi.org/10.3390/catal12121630>

Academic Editor: Nina Kaneva

Received: 8 November 2022

Accepted: 5 December 2022

Published: 12 December 2022

Publisher's Note: MDPI stays neutral with regard to jurisdictional claims in published maps and institutional affiliations.



Copyright: © 2022 by the authors. Licensee MDPI, Basel, Switzerland. This article is an open access article distributed under the terms and conditions of the Creative Commons Attribution (CC BY) license (<https://creativecommons.org/licenses/by/4.0/>).

Abstract: In this work, a g-C₃N₄/porphyrin nanocomposite was fabricated through the self-assembling of monomeric Tetrakis (4-carboxyphenyl) porphyrin (TCPP) molecules with g-C₃N₄ nanomaterials. The characterizing results showed a good distribution of TCPP nanofibers with a diameter of < 100 nm and several micrometers in length on the g-C₃N₄ nanoflakes' surfaces. The prepared g-C₃N₄/porphyrin nanocomposite had two bandgap energies of 2.38 and 2.7 eV, which could harvest a wide range of photon energy in the light spectrum, particularly in visible light. The obtained C₃N₄/TCPP nanocomposite revealed a remarkable photodegradation efficiency toward rhodamine B dyes, with a RhB removing rate of $3.3 \times 10^{-2} \text{ min}^{-1}$. The plausible mechanism for the photocatalytic performance of the g-C₃N₄/porphyrin photocatalyst for the RhB dye's degradation was also studied and discussed.

Keywords: porphyrin-based nanomaterials; C₃N₄/TCPP hybrid material; dye photodegradation; enhanced photocatalysis

1. Introduction

The development of global economics has caused many environmental issues and the discarding of pollutants in wastewater, posing serious threats to human and nature's health [1–3]. Of the various pollutants disposed of in wastewater, organic dyes, originally derived from paper, food, mining, printing leather, and pharmaceutical industries, are highly toxic and contain carcinogenic agents and non-biodegradables. Most common organic dyes found in industrial wastewater can be listed as azo, phenothiazine, and triphenylmethane derivatives [4]. Among these, a commonly used fluorescent label or colorant in industries is rhodamine B (RhB). This organic dye is highly soluble in water and possesses extreme toxicity, being harmful to human health and the environment and posing risks such as teratogenicity, carcinogenicity, and mutagenicity [5–12]. Many strategies have been effectively utilized thus far for removing RhB dye from wastewater, such as redox degradation, photodegradation, coagulation, adsorption, and mixed approaches [13–15]. Each method has various advantages as well as disadvantages. Among them, the photodegradation process has been considered a promising pathway for RhB removal in aqueous media, using photon energy from the solar spectrum [16,17]. However, most photocatalysts for dye degradation can only harvest photon energy in ultraviolet

light due to their large bandgap energy [18]. Therefore, there is an urgency to develop a photocatalyst that is able to absorb photon energy in the visible light region (approximately 42.3% in the solar spectrum).

Organic semiconductor nanostructures with low bandgap energy activated in the visible light region and high absorbing efficiency for photon energy have been extensively employed in photocatalysis. Among organic-based semiconductor photocatalysts, soft solid-state materials constructed from basic organic building blocks of π -conjugated porphyrin derivatives exhibit promising photocatalytic activity [19–25]. Many approaches have been effectively employed to prepare the π -conjugated organic semiconductors for photocatalysis applications [26,27]. Among these, the self-assembly of supramolecules is one of the most used methodologies to design and prepare soft nanostructured materials from monomeric organic molecules, including porphyrin derivatives. Porphyrin-based nanomaterials have been considered a new advanced nanomaterial for many applications, especially in photocatalysis. Porphyrin supramolecular nanostructures are commonly obtained via self-assembly from monomeric molecules and employed as photocatalysts. In order to enhance the photocatalytic activity, porphyrin nanostructures could be incorporated with other inorganic semiconductors to enable photocatalytic efficiency in a wide solar spectrum range and to improve the charge separation. Ionic self-assembly, reprecipitation, and surfactant-assisted self-assembly (SAS) are common self-assembly protocols used for the preparation of porphyrin nanostructures with controlled morphologies [28–31]. Based on each self-assembly technique, porphyrin monomers were designed and synthesized to obtain desired nanostructures. Self-assembled porphyrin nanostructures have been evidenced to be novel photocatalysts for application in environmental treatments [32]. For example, nanostructured porphyrin photocatalysts successfully obtained via self-assembly in the shape of microspheres, octahedra, and nanosheets exhibited remarkable performance for the photodegradation of several organic dyes [33]. However, free-standing nanostructured porphyrin photocatalysts have been hindered from practical application because of their low stability and quick recombining of electrons and holes. Thus, the incorporation of free-standing aggregates with other inorganic semiconductors could be a promising strategy to enhance charge separation, photon energy absorption, and stability. Our group also produced a range of porphyrin-based nanomaterials in regard to incorporate with several inorganic semiconductors, which revealed the enhanced photodegradation efficiency of organic dyes [30,34–37].

With low bandgap energy activated in the visible light region, high chemical and thermal stabilities, graphitic carbon nitride ($g\text{-C}_3\text{N}_4$) is an inorganic semiconductor, which has been extensively studied for photocatalytic applications such as water splitting, pollutant removal, photovoltaic solar cells, and chemical sensors [38–40]. Many approaches are available for the preparation of the $g\text{-C}_3\text{N}_4$ material, including, but not limited to, solution solvothermal methods, microwave heating-assisted approaches, mixing processes, hydrolysis, the sol-gel process, and mechanical grinding [41]. The $g\text{-C}_3\text{N}_4$ -based nanocomposite showed high removal performance toward organic dyes in an aqueous solution [42]. However, a low surface area, fast recombining of generated electrons and holes, and a low photon energy-harvesting capability have limited the use of the $g\text{-C}_3\text{N}_4$ photocatalyst for pollutant degradation in practice [43]. To tackle these disadvantages, $g\text{-C}_3\text{N}_4$ could be doped (metal or nonmetal doping) or incorporated with other semiconductors to improve the photocatalytic efficiency. For example, the $g\text{-C}_3\text{N}_4/\text{NiSO}_4$ nanocomposite was facilely fabricated with a solvent evaporation method, which revealed a rapid removal of rhodamine B (RhB), Congo red (CR), methylene blue (MB), and indigo carmine (IC) under sunlight irradiation [44]. Durga et al. also incorporated $g\text{-C}_3\text{N}_4$ with $\text{Ca}_2\text{Fe}_2\text{O}_5$ to obtain the $g\text{-C}_3\text{N}_4/\text{Ca}_2\text{Fe}_2\text{O}_5$ nanocomposite [45]. The resultant nanocomposite exhibited an improved removal efficiency of up to approximately 96% toward methylene blue. However, most of the semiconductors incorporated with $g\text{-C}_3\text{N}_4$ were inorganic semiconductors; no organic semiconductors have been reported for incorporation with $g\text{-C}_3\text{N}_4$ for enhancing photocatalytic performance.

Herein, we propose a simple strategy to synthesize a g-C₃N₄/porphyrin hybrid material via the self-assembling of TCPP monomers with g-C₃N₄ nanomaterials. The resultant nanocomposite is well-characterized using scanning electron microscopy (SEM), FTIR spectroscopy, X-ray diffraction (XRD), and a UV-Vis spectrophotometer. The photodegradation evaluation of the synthesized nanomaterial was investigated for RhB removal. This work also proposes and discusses the plausible photodegradation mechanism of RhB using the g-C₃N₄/porphyrin photocatalyst.

2. Results and Discussion

The UV-Vis spectrophotometer is a reliable tool for investigating optical characteristics of materials. The optical properties of the TCPP monomers, free-standing assembled TCPP nanofibers, and g-C₃N₄/porphyrin materials were studied with UV-Vis spectra, and the result is shown in Figure 1. The UV-Vis spectra of the monomeric TCPP molecules revealed a sharp peak at approximately 412 nm, which was due to the transition of $a_{1u}(\pi)$ to $e_g^*(\pi)$, which is the absorption of the Soret band. The $a_{2u}(\pi)$ to $e_g^*(\pi)$ transition in porphyrin molecules was also presented, with the appearance of four weak Q-absorption bands ranging from 500 to 700 nm [46,47]. Interestingly, after the self-assembly, a strong peak at approximately 418 nm in the UV-Vis spectra of the TCPP aggregates was observed, which was assigned to the Soret absorption peaks, with a significant decrease in the peak's intensity, which was primarily evident for the self-assembly of the TCPP monomer. The distinct bathochromic and hypsochromic shift in the Soret absorption band from 412 nm to 418 nm (blue shift) before and after the self-assembly indicated the supramolecular assembly of the monomeric porphyrin molecules following the J-type aggregates [31,48,49]. Furthermore, four Q-absorption bands in the monomeric porphyrin molecule transformed into one band at approximately 664 nm after aggregation, which was considered further evidence for the J-type aggregates. After the TCPP monomers self-assembled on the surface of g-C₃N₄ the UV-Vis spectrum of the hybrid material showed similar characteristic peaks, as evidenced in the TCPP aggregates' UV-Vis spectra. The lower intensity of absorption peaks of the hybrid material's UV-Vis spectrum in comparison to that of the TCPP aggregates demonstrated that the TCPP aggregates were well-integrated with the g-C₃N₄ nanomaterials.

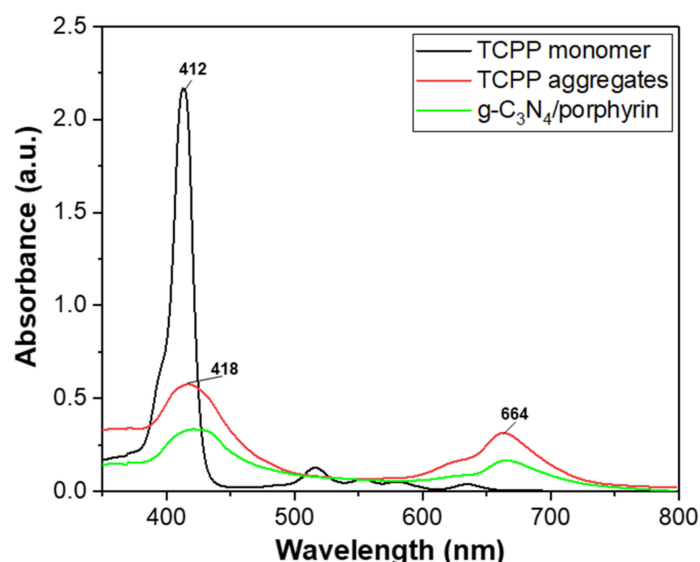


Figure 1. UV-Vis spectra of porphyrin monomer, free-standing self-assembled TCPP, and g-C₃N₄/porphyrin hybrid material.

The morphologies of the free-standing TCPP aggregates, g-C₃N₄, and g-C₃N₄/porphyrin hybrid material were studied using the SEM images (Figure 2). Figure 2a shows the fiber nanostructure of the free-standing TCPP aggregates of less than 100 nm in diameter and

several micrometers in length. The g-C₃N₄ had a flake shape with a nanoscale thickness and a diameter of approximately 0.5 to 2 μm (Figure 2b). Figure 2c,d show the low and high SEM images of the g-C₃N₄/porphyrin. It could be observed that the assembled TCPP nanofibers were uniformly distributed on the surface of the g-C₃N₄ nanoflakes while retaining the morphologies of the free-standing porphyrin nanofibers (Figure 2a) and g-C₃N₄ (Figure 2b). The result was in good agreement with the UV-Vis results, and confirmed the successful synthesis of a well-defined g-C₃N₄/porphyrin hybrid material via self-assembly. The EDS analysis of g-C₃N₄ revealed the atomic percentages of C and N to be 36.62 and 63.38%, respectively, (Figure S1). The self-assembly of g-C₃N₄ with porphyrin witnessed an increase in the C atomic percentage (44.06%) and a decrease in the N atomic percentage (46.22%), as evidenced for the presence of porphyrin in the composite (Figure S2). The O atomic percentage of approximately 8.6% was further evidence of the presence of porphyrin, as it was the main element in the TCPP porphyrin molecules.

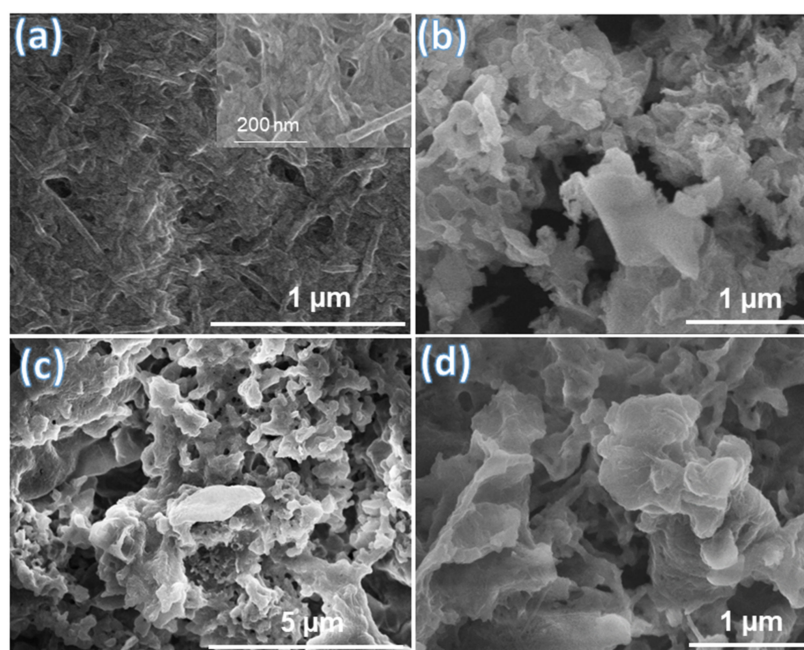


Figure 2. SEM images of (a) free-standing porphyrin aggregates, (b) g-C₃N₄, and (c,d) g-C₃N₄/porphyrin nanofibers.

The bonding nature of the g-C₃N₄/porphyrin hybrid material was investigated with FTIR spectroscopy, and the result is shown in Figure 3. The FTIR spectrum exhibited a broad absorption band in the range of 3000 to 3500 cm^{-1} , which was attributed to the characteristic vibrations of the -OH and -COOH groups in porphyrin molecules and to the moisture. The intense vibration peaks at 1410 and 1640 cm^{-1} were attributed to the C-O and C=O bonds in the carbonyl groups in the porphyrin molecules, respectively [29]. Firm peaks ranging from 1200 to 1650 cm^{-1} were ascribed to the vibrations of the C-N heterocycles, as well as heptazine-derived repeating units [50]. The presence of vibration bands at 1321 and 1242 cm^{-1} were attributed to the stretching vibration modes of the C-NH-C bridge or C-N(-C) trigonal units in g-C₃N₄ [51]. The characteristic vibration of the tri-s-triazine modes was also observed, with the appearance of a stretching band at 812 cm^{-1} . These results further demonstrated that the assembled TCPP porphyrin nanofibers were well-incorporated with the g-C₃N₄ nanoparticles to form a hybrid material. The FTIR spectrum of the monomeric TCPP porphyrin monomers showed similar characteristic vibration bands of porphyrin aggregates in the g-C₃N₄/porphyrin hybrid material, with a small shift, which demonstrated the successful self-assembly of porphyrin monomers into the porphyrin nanofibers.

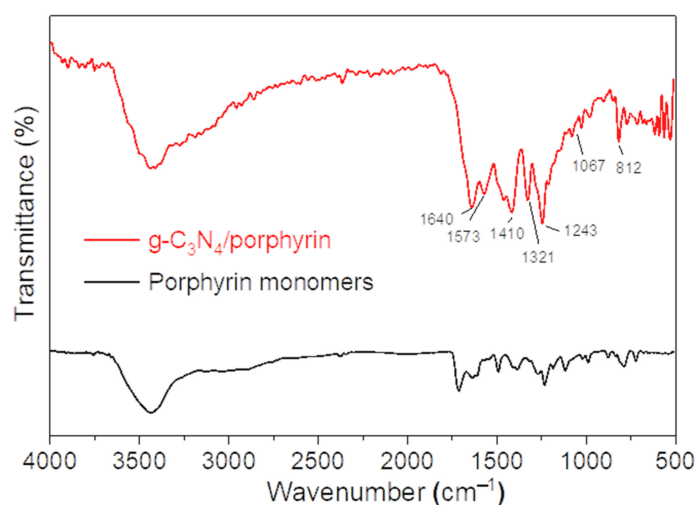


Figure 3. FTIR spectrum of TCPP porphyrin monomer and g-C₃N₄/porphyrin hybrid material.

The phase's characteristics and structure of the hybrid material were studied using the X-ray diffraction (XRD) technique. Illustrated in Figure 4 are the XRD patterns of the prepared samples. The XRD of the monomeric porphyrin molecule revealed no diffraction peaks, conveying the amorphous nature of the porphyrin monomer. The XRD pattern of g-C₃N₄ (black line) depicted diffraction peaks at approximately 13 and 27.8°, which were in good agreement with the g-C₃N₄ material reported previously [52–54]. The strong peak at 27.8° attributed to the plane of (002) in g-C₃N₄ resulted from the layer stacking of the aromatic system. The weak peak at approximately 13° was assigned to the (100) plane (JCPDS NO. 87-1526), which resulted from the tri-s-triazine unit stacking. The XRD pattern of the g-C₃N₄/porphyrin hybrid material also showed characteristic peaks of g-C₃N₄ at approximately 13 and 27.8°. The XRD pattern of the hybrid material showed a small shift in the diffraction peaks of g-C₃N₄, which might be attributed to the electronic interaction between porphyrin and g-C₃N₄. Intriguingly, several additional peaks with an asterisk at two theta values of 19 and 22° were also observed in the hybrid material's XRD pattern, which belonged to the porphyrin aggregates. This result demonstrated the crystalline nature of the porphyrin aggregates [30,36], which was additional confirmation for the successful self-assembling of the TCPP monomer on the surface of g-C₃N₄.

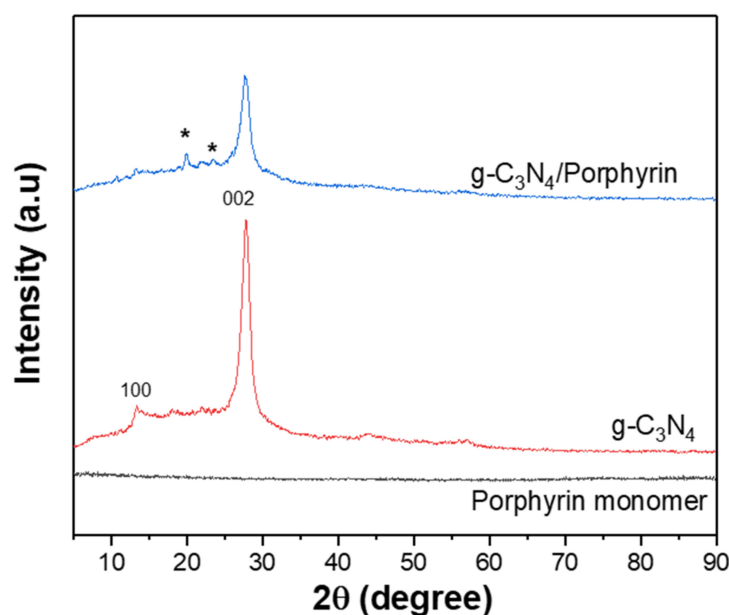


Figure 4. XRD patterns of TCPP porphyrin monomer, g-C₃N₄, and g-C₃N₄/porphyrin material.

The optical properties of the samples were further studied with the diffuse reflectance UV-Vis spectrophotometer. The result is depicted in Figure 5a. The spectrum of the free-standing g-C₃N₄ showed strong absorption in the ultraviolet region (300–400 nm). Interestingly, the diffuse reflectance UV-Vis spectrum of the g-C₃N₄/porphyrin hybrid material showed two broad peaks at approximately 450 nm and 650 nm, indicating that the hybrid material could favorably absorb light in the visible light and near-UV light region. This broad wavelength absorption in the light region was significantly favorable for photocatalytic applications. The difference between the photon energy and bandgaps was responsible for the optical absorption strength of the material, following the below equation:

$$(\alpha h\nu)^{1/n} = A(h\nu - E_g) \quad (1)$$

where E_g is the bandgap energy, α is the coefficient of the absorption band, h is Planck's constant (6.626×10^{-34} Js), ν is the speed of light (3.108×10^8 ms⁻¹), and A is the absorption intensity. The Tauc plot was drawn based on $(\alpha h\nu)^2$ versus $h\nu$, and, then, the bandgap energy of the material was determined using the Tauc plot. Figure 5b shows the Tauc plots of the free-standing g-C₃N₄ and g-C₃N₄/porphyrin hybrid material. The bandgap energies of g-C₃N₄ were calculated from the Tauc plot to be approximately 2.91 eV, only able to harvest the energy of photon energy from ultraviolet light. From the Tauc plot, two bandgap energies of the g-C₃N₄/porphyrin hybrid material were determined to be 2.38 and 2.7 eV, which were favorable for harvesting photon energy from visible and near-ultraviolet light. This result implied that the successful integration of the g-C₃N₄ and TCPP porphyrin aggregates could create a novel photocatalyst with bandgap energies in a wide range of light regions, particularly in visible light.

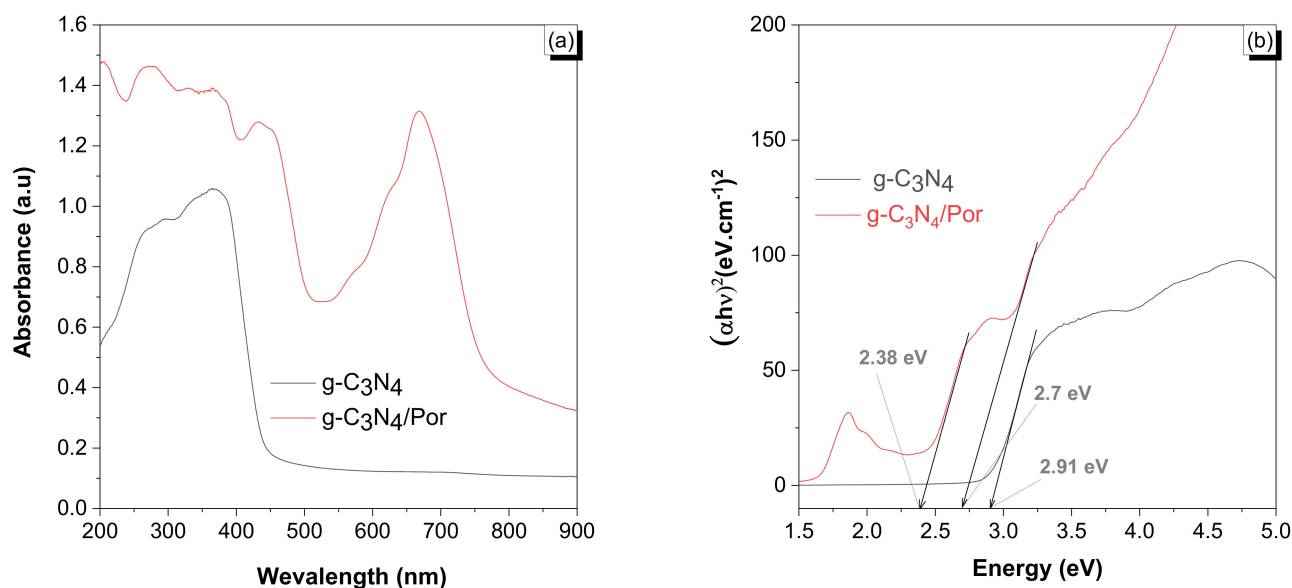


Figure 5. (a) The diffuse reflectance UV-Vis and (b) the Tauc plot of the free-standing g-C₃N₄ and g-C₃N₄/porphyrin hybrid material.

The photodegradation performance of the prepared g-C₃N₄/porphyrin hybrid material was investigated for RhB removal under simulated sunlight irradiation. Figure 6 reveals the effect of the g-C₃N₄ loading on the photodegradation behavior of the hybrid material. It was evident that the photodegradation performance of the g-C₃N₄/porphyrin hybrid material toward RhB was remarkably higher than that of the control, free-standing g-C₃N₄, and TCPP porphyrin aggregates. The RhB removal percentages of the free-standing g-C₃N₄ and TCPP aggregates were determined to be 38 and 42%, respectively, under photocatalytic experimental conditions. When g-C₃N₄ proportions in the g-C₃N₄/porphyrin increased, the photocatalytic degrading efficiency of RhB also increased. At a TCPP:g-C₃N₄ weight ra-

tio of 1:1, the RhB removal percentage was approximately 71%, and enhanced significantly at a ratio of 1:2, with a degrading efficiency of 89%. The RhB degrading efficiency reached a maximum at a TCPP:g-C₃N₄ ratio of 1:3, with a removal percentage of 98%. When the g-C₃N₄ contents further increased, the removal efficiency of the RhB slightly decreased. Thus, the TCPP:g-C₃N₄ ratio of 1:3 was considered to be the optimal proportion of g-C₃N₄ in the hybrid material, and this ratio was selected for the preparation of a hybrid material for further photocatalytic studies.

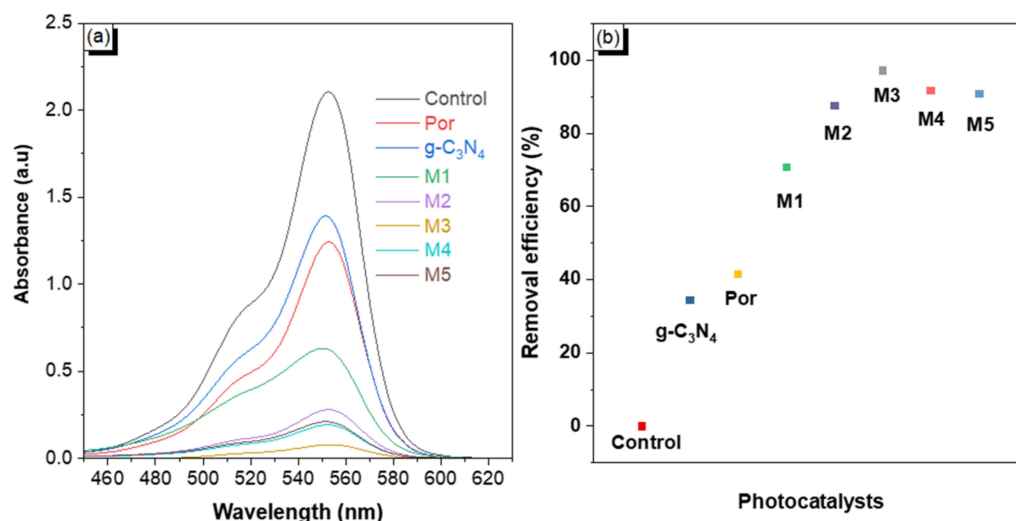


Figure 6. Effect of g-C₃N₄ contents on the photodegradation efficiency of the hybrid material with various TCPP aggregates: g-C₃N₄ weight ratios of 1:1, 1:2, 1:3, 1:4, and 1:6 labeled as M1, M2, M3, M4, and M5, respectively, under simulated sunlight irradiation for 100 min. (a) UV-vis spectra of remaining RhB concentration and (b) removal efficiencies with various photocatalysts.

The g-C₃N₄ with bandgap energies in the range of 2–3 eV has been extensively used as an effective photocatalyst under near-UV and visible light irradiation [55,56]. It has been evidenced that assembled porphyrin has a molecular structure similar to chlorophyll (photoactive molecules), which is a major component participating in many processes of biological energy transduction in algae and plants [57,58]. The bandgap energies of the hybrid material were determined to be 2.38 and 2.7 eV, indicating the effective harvesting of photon energy from a wide range of light regions, especially from the light in the visible light spectrum. Therefore, in this work, photocatalytic experiments were performed for the degradation of RhB using the prepared g-C₃N₄/porphyrin photocatalyst under simulated sunlight irradiation. The result is depicted in Figure 7. It can be seen from Figure 7a that the hybrid material exhibited remarkable photodegradation performance, with a RhB removal efficiency of almost 100% after irradiating with the simulated sunlight for 120 min. Illustrated in Figure 7b is the $\ln(C_t/C_0)$ vs. time plot for studying the photocatalytic reaction's kinetics, in which C_t is the absorption peak's intensity at time t , and C_0 is the absorption peak's intensity at time zero. The photocatalytic performance was evaluated through the changes in the RhB absorption peak at a wavelength of 553 nm as a function of time. Under experimental conditions, the negligible self-sensitized degradation of RhB was observed with no decrease in the concentration of RhB. When free-standing g-C₃N₄ and TCPP porphyrin aggregates were used as photocatalysts, the RhB concentrations remarkably decreased, with a rate constant of cal. 3.75×10^{-3} and $5 \times 10^{-3} \text{ min}^{-1}$, respectively. Intriguingly, when the g-C₃N₄/porphyrin hybrid material was employed as a photocatalyst, the RhB removal percentage remarkably increased, with a rate constant calculated to be approximately $3.3 \times 10^{-2} \text{ min}^{-1}$, which was approximately six- and ten-fold higher compared to the g-C₃N₄ and TCPP aggregates, respectively. In comparison to the other assembled porphyrin-based nanomaterials reported in the literature, this rate

constant for the degradation of RhB using the g-C₃N₄/porphyrin hybrid material was higher, and much higher than the commercial photocatalyst of TiO₂ [30,34,36,59].

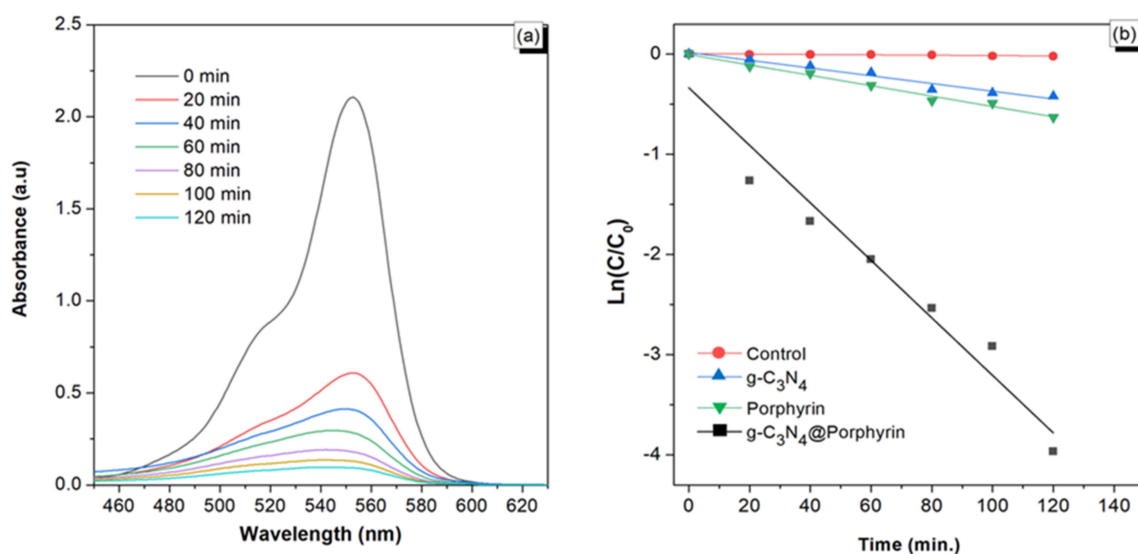


Figure 7. Effect of photocatalytic time on the removal efficiency of RhB using (a) the g-C₃N₄/porphyrin hybrid material prepared with a TCPP:g-C₃N₄ ratio of 1:3 (M3) as the photocatalyst and (b) the kinetics study of the photocatalysts under irradiation of simulated sunlight for 120 min.

It is well-known that J-type porphyrin aggregates are of a photo-semiconductor property, because of their robust π - π intermolecular interactions in the π -conjugate of the porphyrin molecules [20,31,37]. Due to the photo-semiconductor property, porphyrin aggregates via self-assembly can receive energy from photons to enable electrons to move to conduction bands from valence bands and form electron and hole pairs for the photocatalytic reaction [29,49,60]. Additionally, the photocatalytic performance of hybrid materials remarkably increased due to the improvement of charge separation induced through processes of an exciton-coupled charge transfer between the g-C₃N₄ and porphyrin aggregates [61,62]. The g-C₃N₄/porphyrin hybrid material had two bandgap energies of 2.38 and 2.7 eV, which enabled the photocatalyst to receive energy from photons in a wide range of the light spectrum, especially with visible light. Figure 8 proposes the possible photodegrading mechanism of the g-C₃N₄/porphyrin hybrid material for the removal of the RhB organic dye. When g-C₃N₄/porphyrin was irradiated with the sunlight region, the g-C₃N₄ and TCPP nanofibers harvested photon energy to enable the jumping of electrons from the valence band to the conduction band, generating electron/hole pairs [29]. Thanks to processes of the exciton-coupled charge transfer, newly generated electrons diffused from the conduction band of the g-C₃N₄ to the TCPP aggregates, and holes formed the valence band of the TCPP nanofibers to the g-C₃N₄ through the interface between the two materials. These transfer processes significantly avoided the electron and hole recombination; as a result, more electrons and holes could participate in the photocatalysis. Remarkably, the electrons reduced O₂ and H₂O to form free radicals, such as $\cdot\text{O}_2^-$, $\text{OH}\cdot$...; these free radicals oxidized the RhB dye to fewer toxic compounds. The holes also migrated and directly oxidized the RhB molecules to unharmed products.

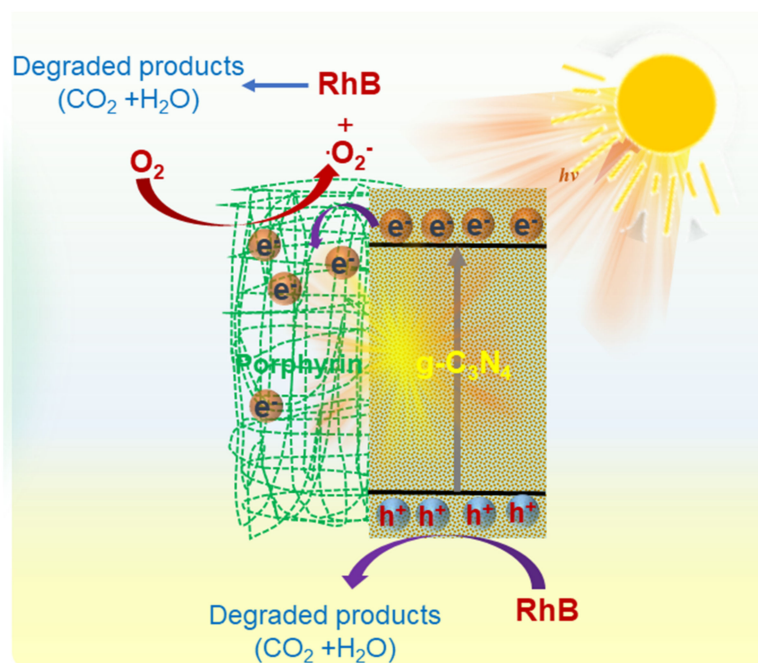


Figure 8. Plausible photodegradation mechanism of the $g\text{-C}_3\text{N}_4$ /porphyrin for the rhodamine B removal.

3. Materials and Methods

3.1. Chemicals

Shanghai Macklin Biochemical Company provided monomeric tetrakis (4-carboxyphenyl) porphyrin (TCPP) molecules. Hydrochloric acid (HCl, 99%), ethanol (99%), sodium hydroxide (NaOH, 99%), and urea ($\text{CH}_4\text{N}_2\text{O}$, 99%) were purchased from Xilong Chemical Co., Ltd., Guangdong, China. All the chemicals without further purification and double-distilled water were employed for all experiments.

3.2. Preparation of $g\text{-C}_3\text{N}_4$ Nanomaterial

The $g\text{-C}_3\text{N}_4$ nanomaterial was prepared through the direct annealing of the urea compound. As in a typical process, a crucible with a cover containing 10 g of urea was heated at 550 °C for 3 h. The crucible was then naturally cooled to room temperature, after which a yellow powder was obtained as raw pristine. The raw $g\text{-C}_3\text{N}_4$ was washed with distilled water several times and ethanol to remove impurities. After that, the sample was completely dried at 70 °C for five hours.

3.3. Synthesis of $g\text{-C}_3\text{N}_4$ /Porphyrin

An acid-based neutralization-induced self-assembly approach was employed to synthesize the $g\text{-C}_3\text{N}_4$ @porphyrin hybrid material. As in a typical process, 8 mg TCPP was dissolved in 2 mL NaOH 0.1M to obtain solution A. Then, different proportions of the $g\text{-C}_3\text{N}_4$ nanomaterial were added into solution A, with various TCPP: $g\text{-C}_3\text{N}_4$ weight ratios of 0.5:1, 1:1, 1:2, 1:4, and 1:6. The resultant mixture was thoroughly mixed for 20 min through bath sonicating to obtain a homogeneous mixture of the $g\text{-C}_3\text{N}_4$ and porphyrin monomers. HCl 0.1M was gradually introduced to the mixture to induce the reprecipitation self-assembly of the porphyrin nanofibers on the surface of $g\text{-C}_3\text{N}_4$. The pH value was then adjusted to a pH of 6–7. The reprecipitates were collected with the use of centrifugation, thoroughly washed with double-distilled water, and dried at 60 °C for 12 h. The samples were stored at room temperature, in ambient humidity for other testing.

3.4. Material Characterization Techniques

The X'Pert PRO PANalytical instrument with a 0.15405 nm Cu-K α radiation source was employed to obtain an X-ray diffraction (XRD) from the investigation of the structure and crystallinity of the C₃N₄@porphyrin hybrid material. Scanning electron microscopy and energy dispersive X-ray spectroscopy (SEM-EDX, Hitachi S-4600, Fukuoka, Japan) were utilized to observe the morphology and the elemental composition of the sample. FTIR spectra were measured in a TENSOR II (Bruker) IR spectrometer by using KBr pellets. A UV-vis spectrophotometer (Jasco V730) in the range of 200–900 nm was used to obtain the optical absorption spectra of the materials. A UV-vis spectrophotometer was also used to study the photodegradation efficiency of the g-C₃N₄@porphyrin hybrid materials to remove RhB dye at an absorption wavelength of 553 nm.

3.5. Photocatalytic Experiments

The photodegradation efficiency of the g-C₃N₄@porphyrin hybrid materials for the removal of a simulated pollutant using RhB organic dye was studied under simulated sunlight irradiation generated from a 350 W xenon lamp (China, 350 W). Following the typical procedure, 0.4 mg of the g-C₃N₄@porphyrin hybrid material was introduced into 20 mL of a 10 ppm RhB solution. The adsorption equilibrium state of the hybrid material was established by placing the mixture in the dark for 2 h, before irradiating with light. The mixture was taken out after each time point and the UV-Vis spectra recorded for each sample. For comparison, the photodegradation performance of the free-standing g-C₃N₄ and TCPP nanofibers in the removal of RhB was obtained following the same photocatalytic protocol with the hybrid material.

4. Conclusions

A facile, self-assembling approach was successfully employed to fabricate the g-C₃N₄/porphyrin hybrid material through self-assembling TCPP porphyrin monomers on g-C₃N₄ nanoflake surfaces. The prepared porphyrin aggregates in a fiber shape of less than 100 nm in diameter and several micrometers in length were shown to be well-integrated in the g-C₃N₄ nanomaterials. The TCPP porphyrin aggregates were determined to form on the g-C₃N₄s via *J*-type self-assembling pathway. The bandgap energies of the g-C₃N₄/porphyrin hybrid material were calculated to be 2.38 and 2.7 eV, which could make the hybrid material an efficient photocatalyst in a broad light spectrum range. Obviously, the hybrid material exhibited an enhanced photodegradation efficiency toward the rhodamine B dye with a degrading speed of up to $3.3 \times 10^{-2} \text{ min}^{-1}$, which was superior to other porphyrin-based photocatalysts reported previously. The enhanced photodegradation efficiency was due to the improved harvesting of photon energy, as well as the enhanced charge separation due to the exciton-coupled charge transfer processes between the g-C₃N₄ and TCPP aggregates. With a facile fabricating method and highly photocatalytic performance, the g-C₃N₄/porphyrin hybrid material is considered an advanced photocatalyst for many applications, such as environmental remediation and water splitting.

Supplementary Materials: The following supporting information can be downloaded at: <https://www.mdpi.com/article/10.3390/catal12121630/s1>, Figure S1: EDS spectrum of the g-C₃N₄; Figure S2: EDS spectrum of the g-C₃N₄/porphyrin.

Author Contributions: Conceptualization: D.D.N., D.D.L. and C.V.T.; methodology: T.T.N., D.D.L. and H.P.N.T.; software: W.J.C. and H.T.L.; investigation: H.T.L., G.T.N., N.T.T. and D.K.N.; data curation: T.T.N. and S.W.C.; writing—original draft: H.T.L. and D.D.L.; writing—reviewing scientific contents and editing: D.D.N., D.D.L. and C.V.T. All authors have read and agreed to the published version of the manuscript.

Funding: This research was funded by the University of Transport and Communications (UTC) under grant number T2022-CB-005.

Data Availability Statement: Not applicable.

Acknowledgments: The authors thank the staff at the Institute of Chemistry and Materials for the support in characterizing and analyses. We also thank the institute for all facilities we used to carry out the work.

Conflicts of Interest: The authors declare no conflict of interest.

References

- Liang, L.; Cheng, L.; Zhang, Y.; Wang, Q.; Wu, Q.; Xue, Y.; Meng, X. Efficiency and mechanisms of rhodamine B degradation in Fenton-like systems based on zero-valent iron. *RSC Adv.* **2020**, *10*, 28509–28515. [\[CrossRef\]](#) [\[PubMed\]](#)
- Sandoval, A.; Hernández-Ventura, C.; Klimova, T.E. Titanate nanotubes for removal of methylene blue dye by combined adsorption and photocatalysis. *Fuel* **2017**, *198*, 22–30. [\[CrossRef\]](#)
- Kumar, S.S.; Kumar, V.; Malyan, S.K.; Sharma, J.; Mathimani, T.; Maskarenj, M.S.; Ghosh, P.C.; Pugazhendhi, A. Microbial fuel cells (MFCs) for bioelectrochemical treatment of different wastewater streams. *Fuel* **2019**, *254*, 115526. [\[CrossRef\]](#)
- Manzoor, J.; Sharma, M. Impact of Textile Dyes on Human Health and Environment. In *Impact of Textile Dyes on Public Health and the Environment*; IGI Global: Hershey, PA, USA, 2020; pp. 162–169.
- Daneshvar, N.; Salari, D.; Khataee, A. Photocatalytic degradation of azo dye acid red 14 in water: Investigation of the effect of operational parameters. *J. Photochem. Photobiol. A Chem.* **2003**, *157*, 111–116. [\[CrossRef\]](#)
- Ledakowicz, S.; Gonera, M. Optimisation of oxidants dose for combined chemical and biological treatment of textile wastewater. *Water Res.* **1999**, *33*, 2511–2516. [\[CrossRef\]](#)
- Nestmann, E.R.; Douglas, G.R.; Matula, T.I.; Grant, C.E.; Kowbel, D.J. Mutagenic activity of rhodamine dyes and their impurities as detected by mutation induction in Salmonella and DNA damage in Chinese hamster ovary cells. *Cancer Res.* **1979**, *39*, 4412–4417.
- Salleh, M.A.M.; Mahmoud, D.K.; Karim, W.A.W.A.; Idris, A. Cationic and anionic dye adsorption by agricultural solid wastes: A comprehensive review. *Desalination* **2011**, *280*, 1–13. [\[CrossRef\]](#)
- Merouani, S.; Hamdaoui, O.; Saoudi, F.; Chiha, M.; Pétrier, C. Influence of bicarbonate and carbonate ions on sonochemical degradation of Rhodamine B in aqueous phase. *J. Hazard. Mater.* **2010**, *175*, 593–599. [\[CrossRef\]](#)
- Mostafa Hosseini Asl, S.; Ghadi, A.; Sharifzadeh Baei, M.; Javadian, H.; Maghsudi, M.; Kazemian, H. Porous catalysts fabricated from coal fly ash as cost-effective alternatives for industrial applications: A review. *Fuel* **2018**, *217*, 320–342. [\[CrossRef\]](#)
- Muhmood, T.; Xia, M.; Lei, W.; Wang, F. Under vacuum synthesis of type-I heterojunction between red phosphorus and graphene like carbon nitride with enhanced catalytic, electrochemical and charge separation ability for photodegradation of an acute toxicity category-III compound. *Appl. Catal. B Environ.* **2018**, *238*, 568–575. [\[CrossRef\]](#)
- Muhmood, T.; Xia, M.; Lei, W.; Wang, F.; Khan, M.A. Efficient and stable ZrO₂/Fe modified hollow-C₃N₄ for photodegradation of the herbicide MTSM. *RSC Adv.* **2017**, *7*, 3966–3974. [\[CrossRef\]](#)
- Bulut, E.; Özacar, M.; Şengil, İ.A. Equilibrium and kinetic data and process design for adsorption of Congo Red onto bentonite. *J. Hazard. Mater.* **2008**, *154*, 613–622. [\[CrossRef\]](#)
- Li, Z.-J.; Wang, L.; Yuan, L.-Y.; Xiao, C.-L.; Mei, L.; Zheng, L.-R.; Zhang, J.; Yang, J.-H.; Zhao, Y.-L.; Zhu, Z.-T. Efficient removal of uranium from aqueous solution by zero-valent iron nanoparticle and its graphene composite. *J. Hazard. Mater.* **2015**, *290*, 26–33. [\[CrossRef\]](#)
- Chen, Z.; Wang, T.; Jin, X.; Chen, Z.; Megharaj, M.; Naidu, R. Multifunctional kaolinite-supported nanoscale zero-valent iron used for the adsorption and degradation of crystal violet in aqueous solution. *J. Colloid Interface Sci.* **2013**, *398*, 59–66. [\[CrossRef\]](#)
- Bhosale, S.V.; La, D.D. Nanoscale porphyrin superstructures: Properties, self-assembly and photocatalytic applications. In *Nanoscience*; Royal Society of Chemistry: London, UK, 2018; pp. 57–85.
- Du, J.; Bao, J.; Liu, Y.; Kim, S.H.; Dionysiou, D.D. Facile preparation of porous Mn/Fe₃O₄ cubes as peroxymonosulfate activating catalyst for effective bisphenol A degradation. *Chem. Eng. J.* **2019**, *376*, 119193. [\[CrossRef\]](#)
- Zhu, X.; Yuan, W.; Lang, M.; Zhen, G.; Zhang, X.; Lu, X. Novel methods of sewage sludge utilization for photocatalytic degradation of tetracycline-containing wastewater. *Fuel* **2019**, *252*, 148–156. [\[CrossRef\]](#)
- Sakakibara, K.; Hill, J.P.; Ariga, K. Thin-Film-Based Nanoarchitectures for Soft Matter: Controlled Assemblies into Two-Dimensional Worlds. *Small* **2011**, *7*, 1288–1308. [\[CrossRef\]](#)
- Würthner, F.; Kaiser, T.E.; Saha-Möller, C.R. J-Aggregates: From Serendipitous Discovery to Supramolecular Engineering of Functional Dye Materials. *Angew. Chem. Int. Ed.* **2011**, *50*, 3376–3410. [\[CrossRef\]](#)
- Zhang, C.; Chen, P.; Dong, H.; Zhen, Y.; Liu, M.; Hu, W. Porphyrin Supramolecular 1D Structures via Surfactant-Assisted Self-Assembly. *Adv. Mater.* **2015**, *27*, 5379–5387. [\[CrossRef\]](#)
- Drain, C.M.; Varotto, A.; Radivojevic, I. Self-organized porphyrinic materials. *Chem. Rev.* **2009**, *109*, 1630–1658. [\[CrossRef\]](#)
- Elemans, J.A.; van Hameren, R.; Nolte, R.J.; Rowan, A.E. Molecular Materials by Self-Assembly of Porphyrins, Phthalocyanines, and Perylenes. *Adv. Mater.* **2006**, *18*, 1251–1266. [\[CrossRef\]](#)
- Hoeben, F.J.; Jonkheijm, P.; Meijer, E.; Schenning, A.P. About supramolecular assemblies of π -conjugated systems. *Chem. Rev.* **2005**, *105*, 1491–1546. [\[CrossRef\]](#) [\[PubMed\]](#)

25. Lee, D.; Kim, K.-D.; Lee, Y.-K. Conversion of V-porphyrin in asphaltenes into V_2S_3 as an active catalyst for slurry phase hydrocracking of vacuum residue. *Fuel* **2020**, *263*, 116620. [\[CrossRef\]](#)
26. Ngai, J.H.; Chan, C.C.M.; Ho, C.H.Y.; Ho, J.K.W.; Cheung, S.H.; Yin, H.; So, S.K. A facile and robust approach to prepare fluorinated polymer dielectrics for probing the intrinsic transport behavior of organic semiconductors. *Mater. Adv.* **2020**, *1*, 891–898. [\[CrossRef\]](#)
27. Marrocchi, A.; Facchetti, A.; Lanari, D.; Petrucci, C.; Vaccaro, L. Current methodologies for a sustainable approach to π -conjugated organic semiconductors. *Energ. Environ. Sci.* **2016**, *9*, 763–786. [\[CrossRef\]](#)
28. Wang, Z.; Medforth, C.J.; Shelnutt, J.A. Porphyrin nanotubes by ionic self-assembly. *J. Am. Chem. Soc.* **2004**, *126*, 15954–15955. [\[CrossRef\]](#)
29. La, D.D.; Bhosale, S.V.; Jones, L.A.; Revaprasadu, N.; Bhosale, S.V. Fabrication of a Graphene@TiO₂@Porphyrin hybrid material and its photocatalytic properties under simulated sunlight irradiation. *ChemistrySelect* **2017**, *2*, 3329–3333. [\[CrossRef\]](#)
30. La, D.D.; Bhosale, S.V.; Jones, L.A.; Bhosale, S.V. Arginine-induced porphyrin-based self-assembled nanostructures for photocatalytic applications under simulated sunlight irradiation. *Photochem. Photobiol. Sci.* **2017**, *16*, 151–154. [\[CrossRef\]](#)
31. Guo, P.; Chen, P.; Ma, W.; Liu, M. Morphology-dependent supramolecular photocatalytic performance of porphyrin nanoassemblies: From molecule to artificial supramolecular nanoantenna. *J. Mater. Chem.* **2012**, *22*, 20243–20249. [\[CrossRef\]](#)
32. La, D.D.; Ngo, H.H.; Nguyen, D.D.; Tran, N.T.; Vo, H.T.; Nguyen, X.H.; Chang, S.W.; Chung, W.J.; Nguyen, M.D.-B. Advances and prospects of porphyrin-based nanomaterials via self-assembly for photocatalytic applications in environmental treatment. *Coord. Chem. Rev.* **2022**, *463*, 214543. [\[CrossRef\]](#)
33. Zhong, Y.; Wang, Z.; Zhang, R.; Bai, F.; Wu, H.; Haddad, R.; Fan, H. Interfacial self-assembly driven formation of hierarchically structured nanocrystals with photocatalytic activity. *ACS Nano* **2014**, *8*, 827–833. [\[CrossRef\]](#)
34. La, D.; Hangarge, R.; Bhosale, S.V.; Ninh, H.; Jones, L.; Bhosale, S. Arginine-mediated self-assembly of porphyrin on graphene: A photocatalyst for degradation of dyes. *Appl. Sci.* **2017**, *7*, 643. [\[CrossRef\]](#)
35. La, D.D.; Rananaware, A.; Salimimarand, M.; Bhosale, S.V. Well-dispersed assembled porphyrin nanorods on graphene for the enhanced photocatalytic performance. *ChemistrySelect* **2016**, *1*, 4430–4434. [\[CrossRef\]](#)
36. La, D.D.; Rananaware, A.; Thi, H.P.N.; Jones, L.; Bhosale, S.V. Fabrication of a TiO₂@porphyrin nanofiber hybrid material: A highly efficient photocatalyst under simulated sunlight irradiation. *Adv. Nat. Sci. Nanosci. Nanotechnol.* **2017**, *8*, 015009.
37. Aljabri, M.D.; La, D.D.; Jadhav, R.W.; Jones, L.A.; Nguyen, D.D.; Chang, S.W.; Dai Tran, L.; Bhosale, S.V. Supramolecular nanomaterials with photocatalytic activity obtained via self-assembly of a fluorinated porphyrin derivative. *Fuel* **2019**, *254*, 115639. [\[CrossRef\]](#)
38. Safaei, J.; Mohamed, N.A.; Noh, M.F.M.; Soh, M.F.; Ludin, N.A.; Ibrahim, M.A.; Isahak, W.N.R.W.; Teridi, M.A.M. Graphitic carbon nitride (g-C₃N₄) electrodes for energy conversion and storage: A review on photoelectrochemical water splitting, solar cells and supercapacitors. *J. Mater. Chem. A* **2018**, *6*, 22346–22380. [\[CrossRef\]](#)
39. Huang, Z.; Zeng, X.; Li, K.; Gao, S.; Wang, Q.; Lu, J. Z-scheme NiTiO₃/g-C₃N₄ heterojunctions with enhanced photoelectrochemical and photocatalytic performances under visible LED light irradiation. *ACS Appl. Mater. Interfaces* **2017**, *9*, 41120–41125. [\[CrossRef\]](#)
40. Malik, R.; Tomer, V.K.; Chaudhary, V.; Dahiya, M.S.; Sharma, A.; Nehra, S.; Duhan, S.; Kailasam, K. An excellent humidity sensor based on In-SnO₂ loaded mesoporous graphitic carbon nitride. *J. Mater. Chem. A* **2017**, *5*, 14134–14143. [\[CrossRef\]](#)
41. Ahmaruzzaman, M.; Mishra, S.R. Photocatalytic performance of g-C₃N₄ based nanocomposites for effective degradation/removal of dyes from water and wastewater. *Mater. Res. Bull.* **2021**, *143*, 111417. [\[CrossRef\]](#)
42. Mohanta, D.; Mahanta, A.; Mishra, S.R.; Jasimuddin, S.; Ahmaruzzaman, M. Novel SnO₂@ZIF-8/gC₃N₄ nanohybrids for excellent electrochemical performance towards sensing of p-nitrophenol. *Environ. Res.* **2021**, *197*, 111077. [\[CrossRef\]](#)
43. Muhmood, T.; Khan, M.A.; Xia, M.; Lei, W.; Wang, F.; Ouyang, Y. Enhanced photo-electrochemical, photo-degradation and charge separation ability of graphitic carbon nitride (g-C₃N₄) by self-type metal free heterojunction formation for antibiotic degradation. *J. Photochem. Photobiol. A Chem.* **2017**, *348*, 118–124. [\[CrossRef\]](#)
44. Yang, S.; Sun, Q.; Han, W.; Shen, Y.; Ni, Z.; Zhang, S.; Chen, L.; Zhang, L.; Cao, J.; Zheng, H. A simple and highly efficient composite based on gC₃N₄ for super rapid removal of multiple organic dyes from water under sunlight. *Catal. Sci. Technol.* **2022**, *12*, 786–798. [\[CrossRef\]](#)
45. Vavilapalli, D.S.; Peri, R.G.; Sharma, R.; Goutam, U.; Muthuraaman, B.; Rao, R.; Singh, S. g-C₃N₄/Ca₂Fe₂O₅ heterostructures for enhanced photocatalytic degradation of organic effluents under sunlight. *Sci. Rep.* **2021**, *11*, 19639. [\[CrossRef\]](#) [\[PubMed\]](#)
46. Sun, J.; Meng, D.; Jiang, S.; Wu, G.; Yan, S.; Geng, J.; Huang, Y. Multiple-bilayered RGO-porphyrin films: From preparation to application in photoelectrochemical cells. *J. Mater. Chem.* **2012**, *22*, 18879–18886. [\[CrossRef\]](#)
47. Chen, Y.; Zhang, C.; Zhang, X.; Ou, X.; Zhang, X. One-step growth of organic single-crystal p-n nano-heterojunctions with enhanced visible-light photocatalytic activity. *Chem. Commun.* **2013**, *49*, 9200–9202. [\[CrossRef\]](#)
48. Guo, P.; Chen, P.; Liu, M. One-dimensional porphyrin nanoassemblies assisted via graphene oxide: Sheetlike functional surfactant and enhanced photocatalytic behaviors. *ACS Appl. Mater. Interfaces* **2013**, *5*, 5336–5345. [\[CrossRef\]](#)
49. Kano, H.; Kobayashi, T. Time-resolved fluorescence and absorption spectroscopies of porphyrin J-aggregates. *J. Chem. Phys.* **2002**, *116*, 184–195. [\[CrossRef\]](#)

50. Lotsch, B.V.; Döblinger, M.; Sehnert, J.; Seyfarth, L.; Senker, J.; Oeckler, O.; Schnick, W. Unmasking melon by a complementary approach employing electron diffraction, solid-state NMR spectroscopy, and theoretical calculations-structural characterization of a carbon nitride polymer. *Chem. A Eur. J.* **2007**, *13*, 4969–4980. [[CrossRef](#)]
51. Liu, J.; Zhang, T.; Wang, Z.; Dawson, G.; Chen, W. Simple pyrolysis of urea into graphitic carbon nitride with recyclable adsorption and photocatalytic activity. *J. Mater. Chem.* **2011**, *21*, 14398–14401. [[CrossRef](#)]
52. Zhou, D.; Qiu, C. Study on the effect of Co doping concentration on optical properties of g-C₃N₄. *Chem. Phys. Lett.* **2019**, *728*, 70–73. [[CrossRef](#)]
53. Li, Y.; Wu, S.; Huang, L.; Wang, J.; Xu, H.; Li, H. Synthesis of carbon-doped g-C₃N₄ composites with enhanced visible-light photocatalytic activity. *Mater. Lett.* **2014**, *137*, 281–284. [[CrossRef](#)]
54. Xu, M.; Han, L.; Dong, S. Facile fabrication of highly efficient g-C₃N₄/Ag₂O heterostructured photocatalysts with enhanced visible-light photocatalytic activity. *ACS Appl. Mater. Interfaces* **2013**, *5*, 12533–12540. [[CrossRef](#)]
55. Liu, X.; Ma, R.; Zhuang, L.; Hu, B.; Chen, J.; Liu, X.; Wang, X. Recent developments of doped g-C₃N₄ photocatalysts for the degradation of organic pollutants. *Crit. Rev. Environ. Sci. Technol.* **2021**, *51*, 751–790. [[CrossRef](#)]
56. Wen, J.; Xie, J.; Chen, X.; Li, X. A review on g-C₃N₄-based photocatalysts. *Appl. Surf. Sci.* **2017**, *391*, 72–123. [[CrossRef](#)]
57. McConnell, I.; Li, G.; Brudvig, G.W. Energy conversion in natural and artificial photosynthesis. *Chem. Biol.* **2010**, *17*, 434–447. [[CrossRef](#)]
58. Barber, J. Photosynthetic energy conversion: Natural and artificial. *Chem. Soc. Rev.* **2009**, *38*, 185–196. [[CrossRef](#)]
59. La, D.D.; Tran, C.V.; Hoang, N.T.; Ngoc, M.D.D.; Nguyen, T.P.; Vo, H.T.; Ho, P.H.; Nguyen, T.A.; Bhosale, S.V.; Nguyen, X.C. Efficient photocatalysis of organic dyes under simulated sunlight irradiation by a novel magnetic CuFe₂O₄@ porphyrin nanofiber hybrid material fabricated via self-assembly. *Fuel* **2020**, *281*, 118655. [[CrossRef](#)]
60. Meadows, P.J.; Dujardin, E.; Hall, S.R.; Mann, S. Template-directed synthesis of silica-coated J-aggregate nanotapes. *Chem. Commun.* **2005**, *29*, 3688–3690. [[CrossRef](#)]
61. Muhmood, T.; Cai, Z.; Lin, S.; Xiao, J.; Hu, X.; Ahmad, F. Graphene/graphitic carbon nitride decorated with AgBr to boost photoelectrochemical performance with enhanced catalytic ability. *Nanotechnology* **2020**, *31*, 505602. [[CrossRef](#)]
62. Muhmood, T.; Xia, M.; Lei, W.; Wang, F.; Khan, M.A. Design of graphene nanoplatelet/graphitic carbon nitride heterojunctions by vacuum tube with enhanced photocatalytic and electrochemical response. *Eur. J. Inorg. Chem.* **2018**, *2018*, 1726–1732. [[CrossRef](#)]